



Magnetoresistance, magnetoimpedance, magnetothermopower, and photoconductivity in silver-doped manganese sulfides

Cite as: J. Appl. Phys. **125**, 175706 (2019); <https://doi.org/10.1063/1.5085701>

Submitted: 14 December 2018 . Accepted: 16 April 2019 . Published Online: 07 May 2019

O. B. Romanova , S. S. Aplesnin , L. V. Udod, M. N. Sitnikov, V. V. Kretinin, K. I. Yanushkevich, and D. A. Velikanov



View Online



Export Citation



CrossMark

Applied Physics Reviews
Now accepting original research

2017 Journal
Impact Factor:
12.894

Magnetoresistance, magnetoimpedance, magnetothermopower, and photoconductivity in silver-doped manganese sulfides

Cite as: J. Appl. Phys. 125, 175706 (2019); doi: 10.1063/1.5085701

Submitted: 14 December 2018 · Accepted: 16 April 2019 ·

Published Online: 7 May 2019



View Online



Export Citation



CrossMark

O. B. Romanova,^{1,2,a)} S. S. Aplesnin,^{1,3} L. V. Udod,^{1,3} M. N. Sitnikov,³ V. V. Kretinin,³ K. I. Yanushkevich,⁴ and D. A. Velikanov¹

AFFILIATIONS

¹Kirensky Institute of Physics, Federal Research Center KSC SB RAS, Krasnoyarsk 660036, Russia

²Department of Engineering Physics and Radio Electronics, Siberian Federal University, Krasnoyarsk 660041, Russia

³Department of Physics, Siberian State University of Science and Technology, Krasnoyarsk 660014, Russia

⁴Scientific-Practical Materials Research Center NAS, Minsk 220072, Belarus

^{a)}E-mail: rob@iph.krasn.ru

ABSTRACT

New multifunction materials in the $\text{Ag}_x\text{Mn}_{1-x}\text{S}$ ($X=0.05$) system have been synthesized and investigated in the temperature range of 77–500 K in magnetic fields up to 12 kOe. Near the temperature of the magnetic transition ($T_N=176$ K), the anomalous behavior of the temperature dependence of magnetization has been observed and has been attributed to the formation of ferrons. An analysis of the infrared spectroscopy data and I - V characteristics has revealed the spin-polaron subband splitting. Several conductivity channels have been found from the impedance spectra. The temperature and magnetic field dependences of the carrier relaxation time have been obtained. The magnetoresistance (−21%), magnetoimpedance (−65%), magnetothermopower (−40%), and photoconductivity effects have been detected. The majority carrier type, density, and mobility have been determined from the Hall-effect measurement data. The observed effects have been explained using a ferron model.

Published under license by AIP Publishing. <https://doi.org/10.1063/1.5085701>

I. INTRODUCTION

Spintronics has been intensively developed for the last few decades.^{1,2} The operation of spintronic devices is based on the colossal magnetoresistive (CMR) effect. In this respect, the highly promising and well-studied materials are manganites.^{3–5} In addition, chalcogenides^{6–8} and their solid solutions^{9–12} were found to be excellent model objects for examining the colossal magnetoresistance.

Despite a great number of works on the CMR effect, most of the available experimental data concern specific properties of materials, including their electrical resistance, magnetoresistance, and thermopower. Meanwhile, the interest in the compounds with the CMR effect is due to the strong interrelation between their magnetic, electron, and elastic subsystems. Therefore, the nature of many effects observed can be understood only via examining their characteristics in their interplay.

Novel microelectronic elements operate on the basis of the spin-dependent electron transport phenomenon. During operation, the spurious thermopower is induced upon heating, which changes its value in a magnetic field. The magnetic thermopower effect observed in some $\text{La}_{1-x}\text{A}_x\text{MnO}_3$ ($A = \text{Ba}, \text{Sr}, \text{etc.}$) manganites^{13,14} was explained by the magnon and phonon drag in the low-temperature region and the hopping polaron charge transfer in the paramagnetic region. Particular attention was focused on the manganites with a giant thermopower of −80% to 100%.^{15,16} In the CuCrTiS_4 chalcogenides, a decrease in the thermopower by a factor of two in a magnetic field of 90 kOe was observed at 5 K, i.e., below the temperature of the spin-glass transition and the Seebeck coefficient, a drop by −26% at $T = 20$ K was found.¹⁷

The Ag-Mn-S manganese chalcogenide-based system has a high application potential and is multifunctional, since it exhibits the four effects: magnetoresistance, magnetoimpedance, magnetic

thermopower, and photoconductivity. A combination of these effects can be used in microelectronic elements, microrefrigerators, and temperature measuring devices for cooling laser diodes, thermal imagers, and night vision equipment.

The initial manganese monosulfide (MnS) in the α modification is an antiferromagnetic acceptor semiconductor ($T_N = 150$ K) with the low (below $0.1 \text{ cm}^2/\text{V s}$) carrier mobility.^{18,19} In the temperature range of 400–450 K, the carrier type changes from hole to electron. Manganese monosulfide with a NaCl-type fcc structure and a unit cell parameter of $a = 5.21 \text{ nm}$ undergoes structural distortions below the Neel temperature.²⁰ Similar to the MnO and NiO oxides, manganese monosulfide is a second-type antiferromagnet with a magnetic unit cell, the sizes of which are twice as much as the crystal unit cell ones. The magnetic moments of Mn^{+2} ions are ferromagnetically ordered in the (111) planes and antiferromagnetically ordered in the neighboring planes.¹⁸ Below the magnetic ordering temperature, the anisotropy of electrical resistance is observed, which is stronger in the (111) plane than in the (100) plane by two orders of magnitude and depends on the applied magnetic field. In MnS, a negative magnetoresistance of 12% in the (111) plane was observed in a magnetic field of 10 kOe at a temperature of $T = 230 \text{ K}$. The enhancement of the resistance anisotropy in the manganese monosulfide below T_N is caused by the interaction of hole spins in the (111) plane and the occurrence of a gap at the Fermi level.^{21,22} The disappearance of the long-range magnetic order in the vicinity of the Neel temperature leads to the positive magnetoresistance and vanishing of the short-range magnetic order at 230 K causes the negative magnetoresistance. Substitution of silver ions for manganese cations evokes hole doping and makes an additional contribution to the exchange coupling between manganese ions as a result of the kinetic s–d interaction and phase separation.²³

The aim of this study was to investigate the effect of nonstoichiometric substitution of silver for manganese on the structural, magnetic, kinetic, and galvanomagnetic properties of the doped manganese sulfide as a result of the s–d interaction using IR spectroscopy.

II. MEASUREMENT TECHNIQUES

The phase composition and crystal structure of the synthesized $\text{Ag}_{0.05}\text{Mn}_{0.95}\text{S}$ samples were studied at room temperature on a DRON-3 X-ray diffractometer ($\text{CuK}\alpha$ radiation) in the pointwise data acquisition mode. In the X-ray diffraction experiment, the 2θ angle range was $3^\circ \leq 2\theta \leq 130^\circ$. The data accumulation time at the 2θ angle point was from $\tau = 3 \text{ s}$ to $\tau = 5 \text{ s}$ and the angle step was $\Delta 2\theta = 0.02^\circ$. The magnetic properties of the $\text{Ag}_{0.05}\text{Mn}_{0.95}\text{S}$ solid solutions were measured on a vibration magnetometer in the temperature range of 77–300 K in magnetic fields up to 10 kOe on the samples cooled in zero (ZFC mode) and nonzero (FC) magnetic fields. The electrophysical properties of the $\text{Ag}_{0.05}\text{Mn}_{0.95}\text{S}$ compounds were investigated in magnetic fields up to 12 kOe at temperatures of 77–400 K in the frequency range of $\omega = 100\text{--}10^6 \text{ Hz}$. The effect of a magnetic field on the transport properties was determined from the I – V characteristics measured at fixed temperatures in a zero magnetic field and in a field of 12 kOe. The resistivity, I – V characteristics, and thermopower were determined on

parallelepiped samples. The thermopower and electrical resistance were measured by two- and four-contact methods in a dc mode at temperatures of 77–500 K in magnetic fields of up to 12 kOe. The thermopower was calculated using the formula $\alpha = U/\Delta T$, where U is the potential difference between the hot and cold sample ends. The Hall voltage was measured in a dc mode at temperatures of 100–400 K in a magnetic field of 12 kOe. In the measurements, the contributions of spurious voltages caused by the side galvanomagnetic and thermomagnetic effects, as well as the contact asymmetry (ZFC measurements), were taken into account.

In this work, we studied and identified the structure of IR spectra of the $\text{Ag}_{0.05}\text{Mn}_{0.95}\text{S}$ solid solutions using an FSM 2202 Fourier spectrometer. The measurements were performed in an optical cryostat in the temperature range of 77–500 K on $\text{Ag}_{0.05}\text{Mn}_{0.95}\text{S} + \text{KBr}$ tablets 10–20 mm in diameter. The photoconductivity was measured by a two-contact method. The photo surface between contacts was exposed to visible light and IR radiation. The duration of resistivity measurements under illumination was $\sim 1 \text{ min}$. A halogen lamp was used as a light source. During the experiments, the luminous power of the lamp was kept constant.

III. SYNTHESIS, STRUCTURE, AND MAGNETIC PROPERTIES

The $\text{Ag}_X\text{Mn}_{1-X}\text{S}$ ($X = 0.05$) crystals were grown for the first time from a melt of polycrystalline sulfide powders in a quartz reactor. The crystallization mixture consisted of calculated amounts of manganese and silver sulfides prepared by sulfidizing the metal oxides by the NH_4SCN thermolysis products at temperatures of 850–1000 °C. The process completeness was controlled using an X-ray diffraction analysis and weighting a glassy carbon container with the substance to a constant weight. The $\text{Ag}_X\text{Mn}_{1-X}\text{S}$ compound was crystallized from the sulfide melt in an inert atmosphere in graphite or glassy carbon containers by drawing the quartz reactor through an inductor at a rate of 5–10 mm/h. The crystallization conditions were established experimentally. The obtained crystals were cylinders $10 \times 30 \text{ mm}^2$ in size, which had a weight of about 6 g.

According to the X-ray diffraction (XRD) data, the $\text{Ag}_X\text{Mn}_{1-X}\text{S}$ ($X = 0.05$) solid solutions consist of two phases (Fig. 1): NaCl-type cubic typical of the initial manganese monosulfide MnS and monoclinic typical of silver sulfide α - Ag_2S (acanthite).²⁴ The cation substitution leads to an increase in the unit cell parameter a from 0.522 nm for α -MnS²¹ to 0.523 nm for the $\text{Ag}_{0.05}\text{Mn}_{0.95}\text{S}$ composition, in accordance with an increase in the substitute ionic radius ($r = 0.091 \text{ nm}$ for Mn and $r = 0.113 \text{ nm}$ for Ag). The growth of the crystal lattice parameter shows that a part of silver is involved in the cation substitution. This substitution leads to the shift of reflections of the main manganese sulfide phase from the initial position toward smaller angles by 0.7° . After the cationic substitution of silver for manganese, the reflections of the main phase of manganese monosulfide shift by 0.7° toward smaller angles from their initial position. The XRD patterns contain, along with the (200), (220), (400), (422), and (442) reflections of the cubic structure typical of manganese monosulfide, a series of weak-intensity reflections typical of Ag_2S . The presence of the second phase in the investigated sample against the MnS background is established by additional reflections and a noticeable broadening of

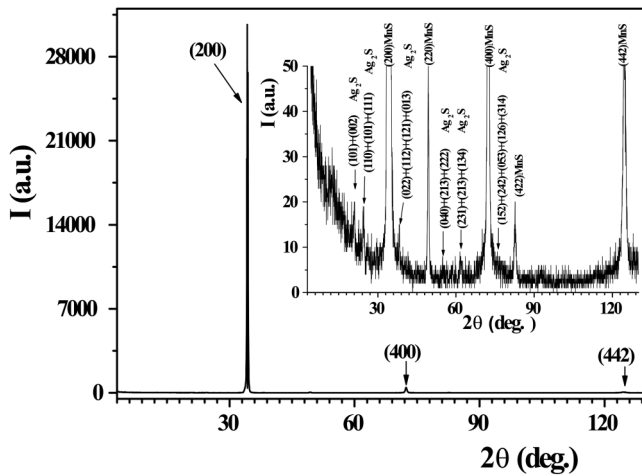


FIG. 1. X-ray diffraction patterns of the $\text{Ag}_{0.05}\text{Mn}_{0.95}\text{S}$ solid solution at $T = 300$ K. Inset: identification of the Ag_2S reflections.

the bases of the primary phase reflections, which are indicative of the MnS crystal structure strain. In addition, the broadening of the reflection bases evidences for the similarity of the 2θ angles of the second-phase reflections superimposed on the primary-phase reflections. The XRD patterns (inset in Fig. 1) allow one to identify additional second-phase reflections with the Ag_2S monoclinic structure [sp. gr. S.G.: $P2_1/n$ (14)]. No reflections corresponding to Ag were observed. The stoichiometric analysis of the $\text{Ag}_{0.05}\text{Mn}_{0.95}\text{S}$ solid solutions showed that the obtained crystals are almost free of oxygen inclusions within the experimental error and only the minor sulfur nonstoichiometry is observed. The nonstoichiometric substitution of silver for manganese in the $\text{Ag}_x\text{Mn}_{1-x}\text{S}$ system leads to the occurrence of anionic vacancies in accordance with the electroneutrality principle.

Figures 2(a) and 2(b) show temperature dependences of the magnetization of the $\text{Ag}_{0.05}\text{Mn}_{0.95}\text{S}$ samples. The magnetization curves are typical of antiferromagnets. The $\sigma(T)$ maximum [Fig. 2(a)] is related to the antiferromagnetic transition at $T_N = 176$ K, which shifts toward higher temperatures relative to the initial manganese monosulfide ($T_N = 150$ K). The absolute value of the paramagnetic Curie temperature $\Theta = -326$ K of the $\text{Ag}_{0.05}\text{Mn}_{0.95}\text{S}$ compound decreases relative to $\Theta = -450$ K for MnS .²⁵ Manganese monosulfide and MnS -based solid solutions with a concentration of $X \leq 0.05$ are characterized by the second-type magnetic ordering $\Theta = \frac{2}{3}S(S+1)(Z_1J_1 + Z_2J_2) = A(12J_1 + 6J_2)$; $T_N = A6J_2$, where $J_{1,2}$ are the exchange couplings in the first and second coordination spheres with number $Z_{1,2}$ of the nearest neighbors. Thus, the cation substitution of silver for manganese will decrease the J_1 value.²⁶ In the Neel temperature region and below it, the $\text{Ag}_{0.05}\text{Mn}_{0.95}\text{S}$ sample exhibits the irreversible magnetization behavior upon sample cooling in a magnetic field of 100 Oe and in the ZFC mode [Fig. 2(a)]. This is indicative of the fact that in weak magnetic fields the solid solution is not a homogeneous antiferromagnet below the magnetic transition temperature. With an increase in the magnetic field to 10 kOe, the magnetization curves coincide [Fig. 2(b)] and an $\sigma(T)$ anomaly

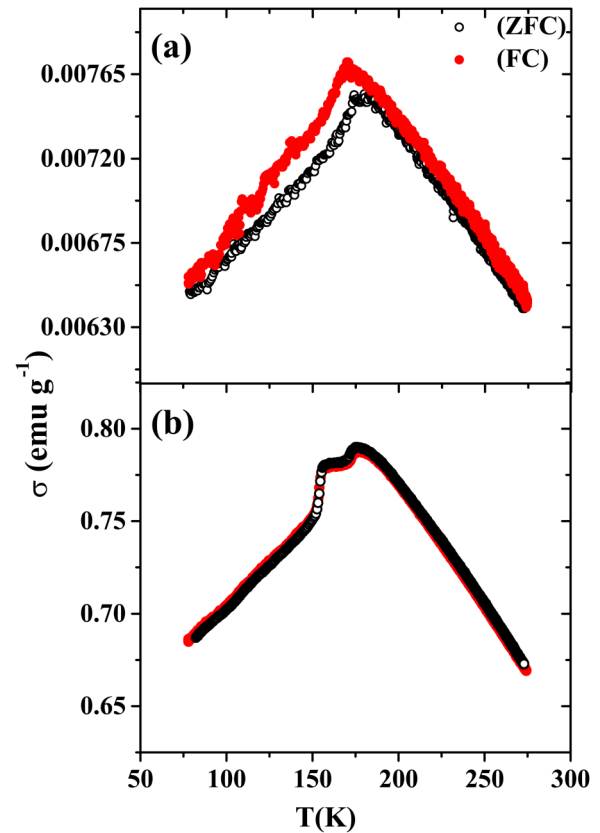


FIG. 2. Temperature dependences of magnetization for the $\text{Ag}_{0.05}\text{Mn}_{0.95}\text{S}$ solid solution measured in a magnetic field of (a) $H = 100$ Oe and (b) 10 kOe upon cooling in zero (ZFC) and nonzero (FC) magnetic fields.

arises at 160 K near the temperature of the magnetic transition. The anomalous behavior of the temperature dependences of magnetization of the $\text{Ag}_{0.05}\text{Mn}_{0.95}\text{S}$ solid solution around the magnetic transition temperature can be attributed to the formation of ferromagnetic droplets (ferrons) in the antiferromagnetic matrix.²³ Conduction electrons are frozen in the antiferromagnetic sublattices below T_N with the formation of ferromagnetic ordering in the local region. In a magnetic field, the magnetic moment of a ferromagnetic droplet tends to align parallel to the field, which leads to an increase in the magnetization. The exchange energy of a droplet with the antiferromagnetic matrix decreases upon heating and, in a strong magnetic field, the droplet magnetic moment can change its orientation, which causes the $\sigma(T)$ jump.

IV. MAGNETOIMPEDANCE AND MAGNETORESISTANCE

The trend to the phase separation in the low-temperature region and change in the electronic spectrum under the s - d interaction of electrons and the chemical potential shift modify the electrical properties of the compound. Figure 3 illustrates the temperature

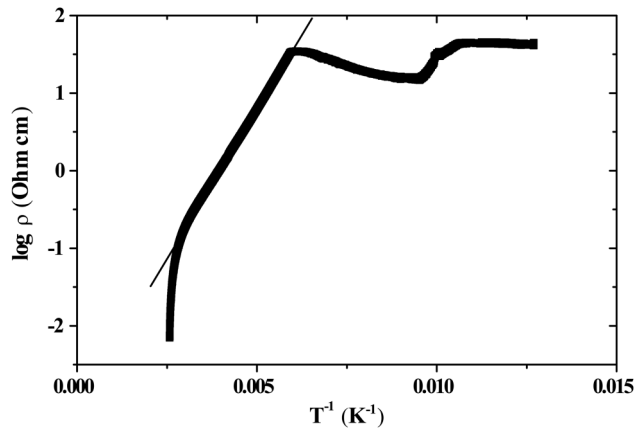


FIG. 3. Temperature dependence of the resistivity of the $\text{Ag}_{0.05}\text{Mn}_{0.95}\text{S}$ solid solution measured in a zero magnetic field.

behavior of the resistivity of the $\text{Ag}_{0.05}\text{Mn}_{0.95}\text{S}$ solid solution. The resistivity of the initial manganese monosulfide is $\rho \sim 10^8 \Omega \text{ cm}$ in the antiferromagnetic region and $\rho \sim 10^4 \Omega \text{ cm}$ in the paramagnetic region at $T = 300 \text{ K}$. As a result of the cationic substitution of silver for manganese, the resistivity in the low-temperature region drops by six orders of magnitude (Fig. 3). The $\rho(T)$ dependence includes a small region at $T \leq 93 \text{ K}$ where the resistance is almost temperature-independent and decreases stepwise at 110 K . The sharp resistivity change is caused by the lattice strain in the initial manganese monosulfide.²⁰ The resistivity measurements showed a pronounced maximum at 160 K near the magnetic transition temperature, which is consistent with the $\sigma(T)$ maximum in a magnetic field [Fig. 2(b)]. The resistivity growth upon heating in the magnetically ordered region is related to the enhanced scattering of spin polarons on the magnetic-order fluctuations. At temperatures of $T > 160 \text{ K}$, the resistivity smoothly decreases with an activation energy of $E_a = 0.14 \text{ eV}$, which is lower than the value for MnS ($E_a = 0.19 \text{ eV}$) in this temperature range.¹⁸ As the temperature increases, the spin-polaron band vanishes and a narrow impurity subband occurs; the conductivity is implemented via the transition of electrons from the valence to the impurity subband.

The ferron-type inhomogeneous electronic state can be detected using the impedance spectroscopy technique. Figures 4(a), 4(b), and 4(c) show impedance hodographs for the $\text{Ag}_{0.05}\text{Mn}_{0.95}\text{S}$ solid solutions measured without magnetic field and in a field of $H = 12 \text{ kOe}$. The equivalent circuit approximation analysis of the impedance spectra allowed us to extract the contributions to the conductivity by temperature and frequency. In the temperature range of $T < 120 \text{ K}$, the hodograph represents a semicircle. Such a hodograph corresponds to the parallel RC contour. In the temperature range of $120\text{--}170 \text{ K}$ in the vicinity of the magnetic transition, the impedance hodograph includes two pronounced arcs in a zero magnetic field, which can be described by a circuit consisting of series RC contours of the high- (R_H, C_H) and low-frequency (R_L, C_L) regions [Fig. 4(b)]. The linear portion in the high-frequency region corresponds to the diffusion

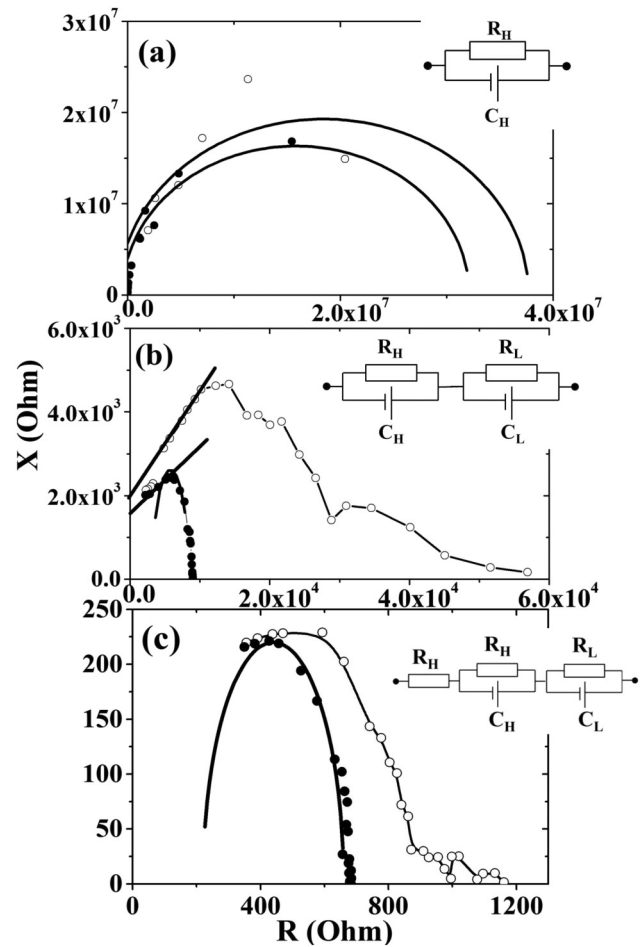


FIG. 4. Hodographs measured in a zero magnetic field (white circles) and in a field of 12 kOe (black circles) at $T =$ (a) 80 , (b) 160 , and (c) 200 K . Lines show the approximation of the equivalent circuit for the low- and high-frequency regions. Inset: equivalent circuit used to simulate the high-frequency resistance and capacitance (R_H and C_H) and low-frequency resistance and capacitance (R_L and C_L). Straight lines in Fig. 4(b) show the diffusion contribution estimated in terms of the Warburg model.

contribution described by the Warburg impedance for elements with a finite diffusion length. The diffusion contribution is related to the increase in the carrier mobility in a magnetic field in the vicinity of the magnetic phase transition. As the temperature increases ($T > 170 \text{ K}$), the high-frequency spectrum portion is modified and resistance R_H is added to the circuit of series contours. To determine the carrier relaxation time, we analyze below the frequency dependences of the real and imaginary parts of the total impedance.

Figures 5(a) and 5(b) show frequency dependences of the active and reactive resistances measured in the temperature range of $80\text{--}320 \text{ K}$ in a magnetic field of 12 kOe and without field. With an increase in temperature, the active (R) and reactive (X) resistances

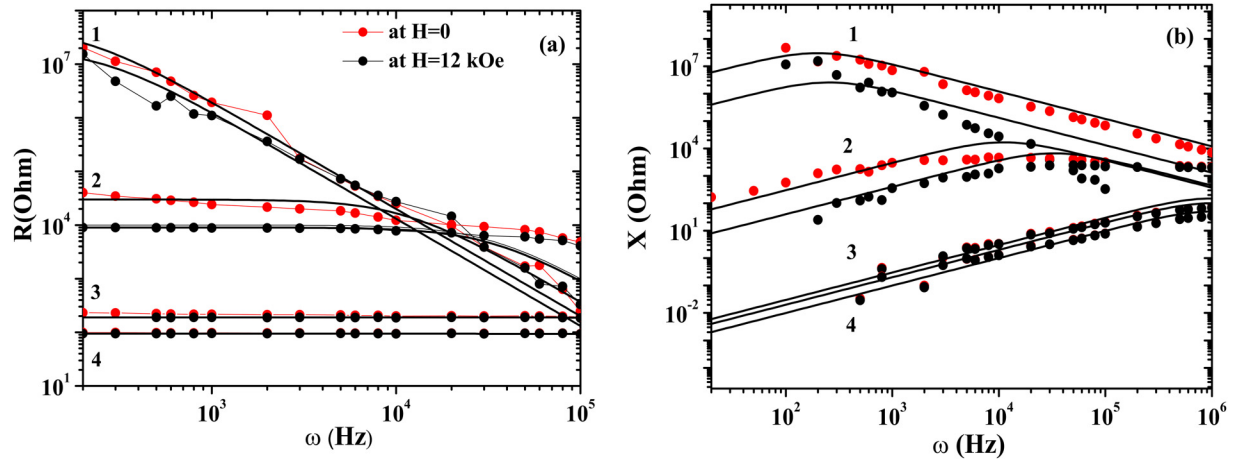


FIG. 5. Frequency dependence of (a) the active and (b) reactive resistances of the $\text{Ag}_{0.05}\text{Mn}_{0.95}\text{S}$ solid solution measured in a zero field and in a magnetic field of $H = 12$ kOe at $T = (1) 80, (2) 160, (3) 240,$ and $(4) 280$ K. The lines show Debye model fitting functions.

decrease in the absolute value and their frequency dependences change. The $X(\omega)$ maximum shifts to the high-temperature region and, above 300 K, goes beyond the measurement range. In the low-frequency region, the real part of the impedance slightly exceeds the imaginary part. The maximum change in the real part of the impedance in the low-frequency region is observed in the vicinity of the magnetic transition temperature and above it, where it is larger than the imaginary part by 2–4 orders of magnitude.

The maximum impedance change $\delta(Z) = \frac{Z(H) - Z(0)}{Z(0)}$ in a magnetic field is $\sim 75\%$ in the magnetic transition region at low frequencies [Fig. 6(a)]. With an increase in frequency, the magnetoimpedance decreases and, at $\omega = 10^6$ Hz, amounts to $\sim 11\%$. At $T > 220$ K, the magnetoimpedance is no more than $\sim 2\%$ over the entire frequency range. The frequency dependences of the real and

imaginary parts of the impedance [Figs. 5(a) and 5(b)] are described well by the Debye model at $\omega > 10^2$ Hz

$$\text{Re } Z(\omega) = \frac{A}{1 + (\omega\tau)^2}, \quad \text{Im } Z(\omega) = \frac{B\omega\tau}{1 + (\omega\tau)^2}, \quad (1)$$

where A and B are the parameters, which are constant and temperature-independent, and τ is the relaxation time. Figure 6(b) illustrates the relaxation time, which decreases in a magnetic field and with increasing temperature. In the region of the magnetic phase transition, the relaxation time decreases due to the energy transfer to the spin subsystem. Below 120 K, the ferron diffusion weakens and the magnon contribution prevails. Above the

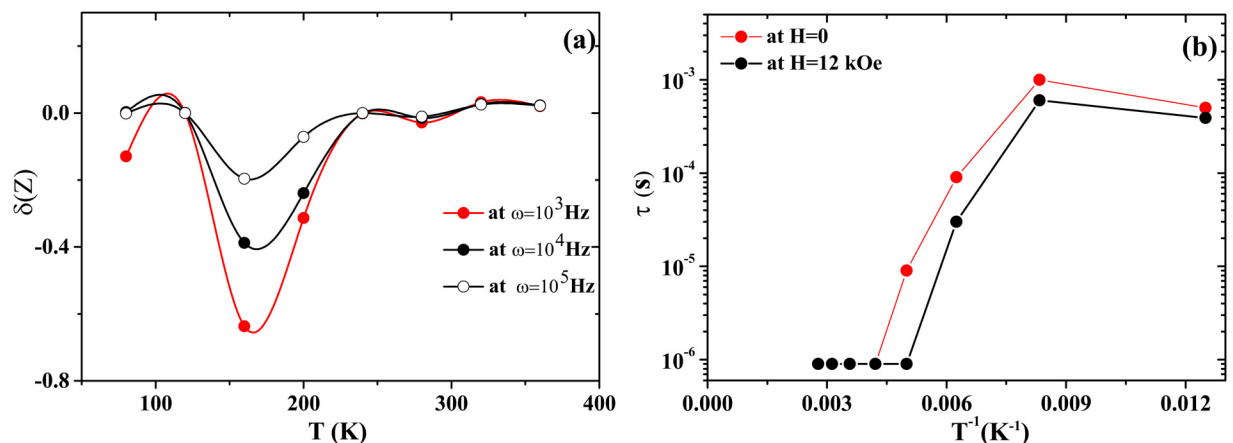


FIG. 6. Temperature dependences of (a) magnetoimpedance $\delta(Z) = \frac{Z(H=12\text{kOe}) - Z(H=0)}{Z(H=0)}$ at frequencies of $\omega = 10^3, 10^4,$ and 10^5 Hz and (b) relaxation time for the $\text{Ag}_{0.05}\text{Mn}_{0.95}\text{S}$ solid solution measured in a zero field and in a field of 12 kOe.

temperature of the magnetic transition, the ferron density decreases and the relaxation time stabilizes.

The electrically inhomogeneous ferron-type states manifest themselves in the I - V characteristics. Figures 7(a)–7(c) show I - V characteristics of the polycrystalline $\text{Ag}_{0.05}\text{Mn}_{0.95}\text{S}$ samples measured without field and in a field of 12 kOe. Below the temperature of the magnetic transition, the I - V characteristics are nonlinear, which is related to the electron hoppings between ferrons. The conductivity is implemented via these hoppings. The electron should overcome the energy barrier caused by the Coulomb interaction

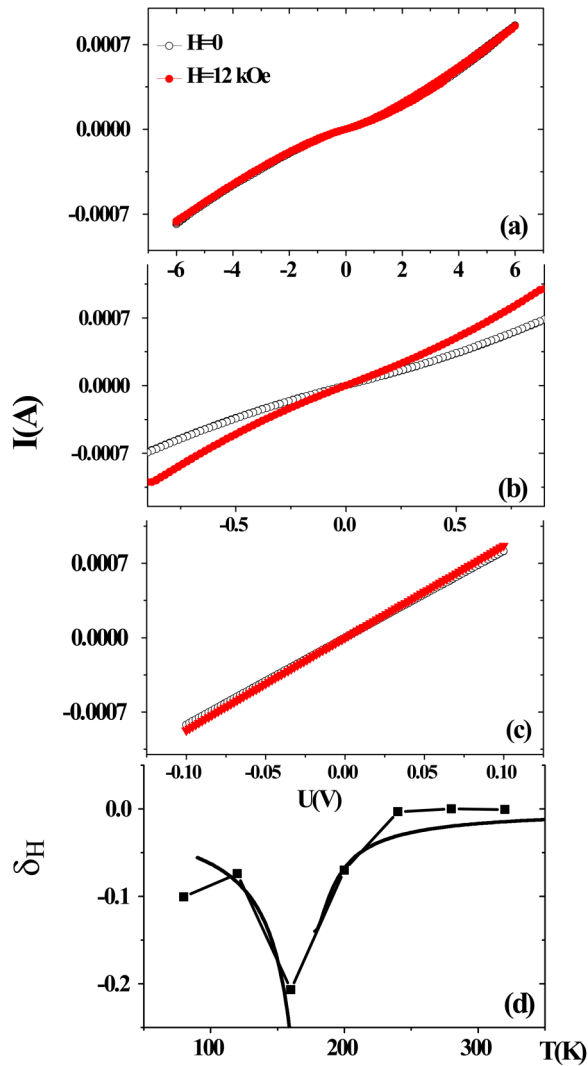


FIG. 7 I - V characteristics of the $\text{Ag}_{0.05}\text{Mn}_{0.95}\text{S}$ solid solution measured in a zero magnetic field and in a field of 12 kOe at T = (a) 80, (b) 160, and (c) 280 K. (d) Temperature dependence of magnetoresistance $\delta_H = \frac{R(H=12\text{kOe}) - R(H=0)}{R(H=0)}$. The fitting was made using Eq. (2) at $H = 12$ kOe, $B = 0.09 \text{ T}^{-1}$ at $T > T_N$, and $B = 0.028 \text{ T}^{-1}$ at $T < T_N$.

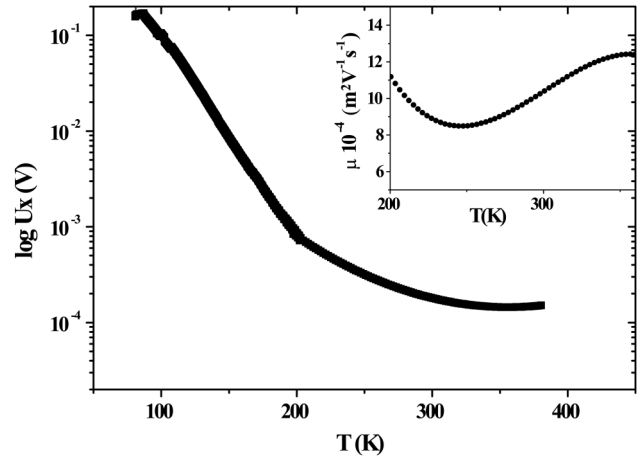


FIG. 8 Temperature dependence of the Hall voltage for the $\text{Ag}_{0.05}\text{Mn}_{0.95}\text{S}$ solid solution. Inset: temperature dependence of the current carrier mobility.

$A = \frac{e^2}{\epsilon R_{\text{fer}}}$, where ϵ is the static permittivity and R_{fer} is the ferron radius. When ferrons vanish, the I - V characteristics stay linear with increasing temperature and are almost field-independent. The magnetoresistance δ_H calculated using the formula $\delta_H = \frac{R(H) - R(0)}{R(0)}$, where $R(H)$ is the resistivity in a magnetic field and $R(0)$ is the resistivity without field, is negative in a wide temperature range [Fig. 7(d)]. At low temperatures, the resistance decreases in a magnetic field and the magnetoresistance (-21%) and magnetoimpedance have the maximum absolute values near the temperature of the magnetic transition. Above the Neel temperature, the resistance decreases in a magnetic field and, at $T \geq 220$ K, amounts to about -0.1% . The magnetoresistance of the semiconductors, the conductivity of which is described by the ferron model,²⁷ obeys the

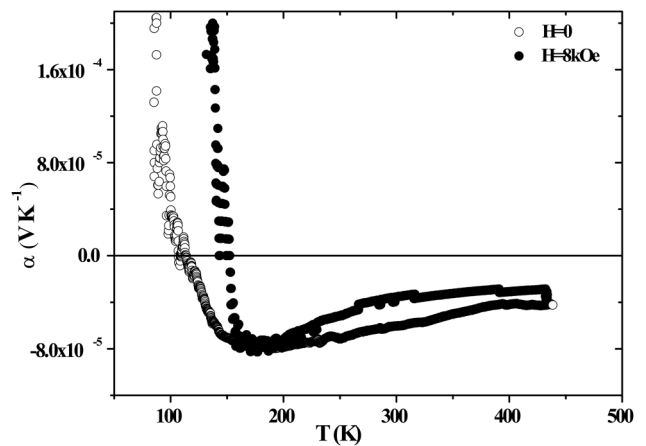


FIG. 9 Temperature dependence of thermopower coefficient α in a zero field and in a magnetic field of $H = 8$ kOe.

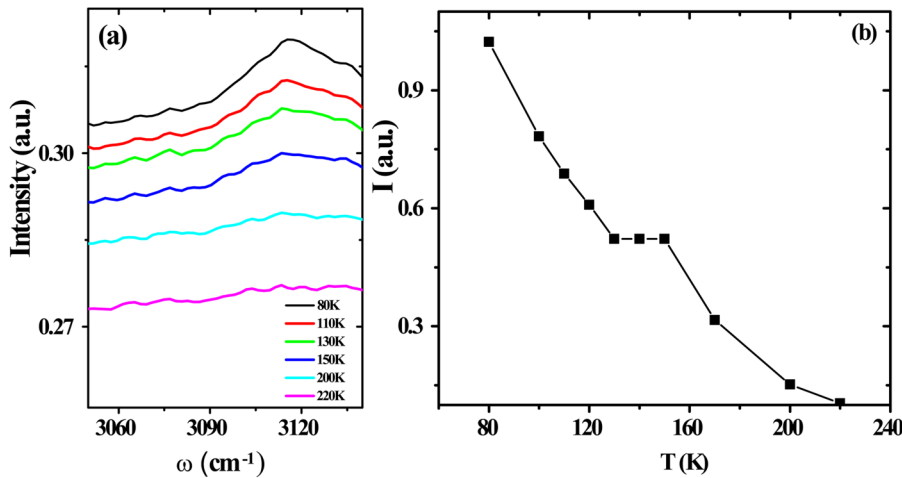


FIG. 10. (a) IR spectra for the polycrystalline $\text{Ag}_{0.05}\text{Mn}_{0.95}\text{S}$ sample at temperatures of 80, 110, 130, 150, 200, and 220 K. (b) Temperature dependence of the peak intensity in the IR spectra at frequency $\omega \sim 3118 \text{ cm}^{-1}$.

exponential law

$$\frac{\rho(H) - \rho(0)}{\rho(0)} = \exp(-BH\xi) - 1 = \exp\left(-\frac{BH}{\left|1 - \frac{x}{T_N}\right|}\right) - 1, \quad (2)$$

where B is the parameter, H is the external magnetic field, and $\xi = 1/[1 - T/T_N]$ is the electron localization radius.^{28,29} The experimental data on magnetoresistance are satisfactorily described using this model in a field of $H = 12 \text{ kOe}$ at $B = 0.09 \text{ T}^{-1}$ at $T > T_N$ and $B = 0.028 \text{ T}^{-1}$ in the magnetically ordered region. Fitting functions are shown by a solid line in Fig. 7(d).

V. MAGNETOTHERMOPOWER AND HALL EFFECT

The inhomogeneous electric and magnetic states can be observed when studying the galvanomagnetic properties.

Figure 8 shows the temperature dependence of the Hall voltage, which includes two portions, below and above the temperature of the magnetic phase transition. In the paramagnetic region, we estimated the carrier (hole) density using the relation $R_X = 1/ne$ and found it to be $n = 10^{19} - 10^{20} \text{ cm}^{-3}$. The majority carrier mobility smoothly increases with temperature (inset in Fig. 8). Upon approaching the magnetic ordering temperature, the Hall resistance is added with an anomalous part caused by the sublattice magnetization $R_H = R_0B + R_S M$, where R_0 and R_S are the normal and anomalous (spontaneous) Hall constants, B is the magnetic induction in the sample, and M is the sublattice magnetization.³⁰ In manganese sulfide, the resistance anisotropy in the (111) plane and along the (100) cube edges was established below the Neel temperature. This phenomenon was attributed to the ferromagnetic ordering of spins in the (111) plane.²¹ The magnetization growth leads to an increase in the Hall resistance and thermopower.

Figure 9 presents the temperature dependence of the thermopower α in a zero magnetic field and in a field $H = 8 \text{ kOe}$. In contrast to the Hall voltage, the thermopower changes its sign at $T = 115 \text{ K}$ in the zero field; in the nonzero magnetic field, this temperature

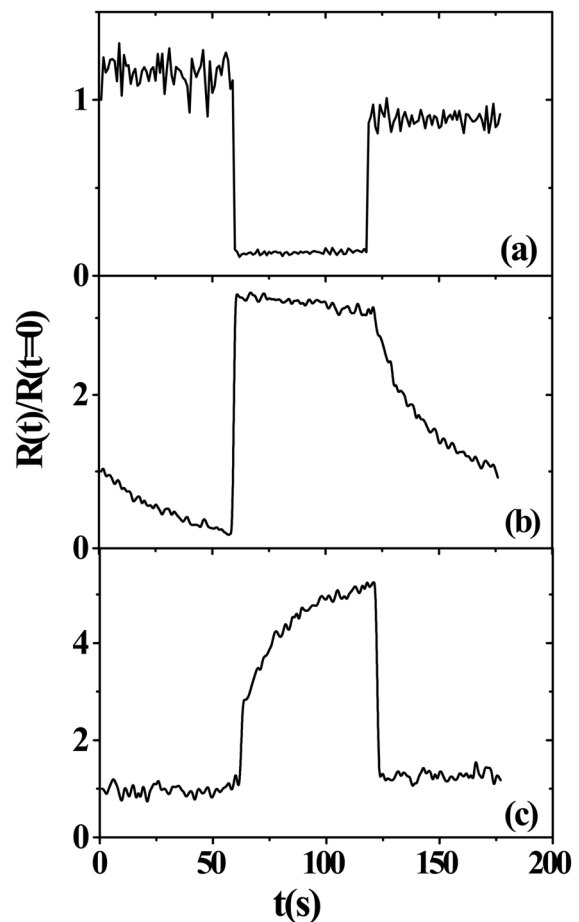


FIG. 11. Normalized resistance of the $\text{Ag}_{0.05}\text{Mn}_{0.95}\text{S}$ solid solution unirradiated (1st minute) and irradiated in the IR (2nd minute) and visible range (3rd minute) at temperatures of $T =$ (a) 80, (b) 200, and (c) 280 K.

shifts to 150 K and the thermopower increases. In the magnetically ordered region, the energy is transferred by electrons dragged by magnons, which leads to an increase in the thermopower. In a magnetic field, the carrier mobility increases due to the suppression of spin fluctuations.

In the paramagnetic region, the absolute value of the thermopower smoothly decreases upon heating and, in a magnetic field, attains -40% near room temperature. It can be related to the existence of two types of energy carrier (holes and excitons). Since there is no magnetoresistance in this temperature range, the main contribution to the magnetothermopower is made by excitons, which consist of electrons and holes with different mobilities. This induces the Lorentz force, which acts on excitons in a magnetic field.

VI. IR SPECTRUM AND PHOTORESISTIVE EFFECT

Using IR spectroscopy, we determined the impurity subband splitting. The IR spectra of the $\text{Ag}_{0.05}\text{Mn}_{0.95}\text{S}$ solid solution were measured at temperatures of 80–550 K in the frequency range of $3060\text{--}3140\text{ cm}^{-1}$; at $\omega \sim 3118\text{ cm}^{-1}$, the peak was observed [Fig. 10(a)]. The peak maximum shifts in frequency from 3118 cm^{-1} at $T = 80\text{ K}$ to 3114 cm^{-1} at $T = 200\text{ K}$. Below the magnetic ordering temperature, the impurity subband splits due to the $s\text{--}d$ interaction, and the transition of electrons from the lower to the upper subband is related to the IR radiation absorption. At $T > 200\text{ K}$, the IR spectral peak vanishes. At these temperatures, the subband is not split, which is consistent with the impedance spectroscopy data.

The transition of electrons from the lower to the upper subband enhances the carrier density and mobility and reduces the resistance. In particular, under IR irradiation, the resistance decreases by a factor of three, while, in the visible range, it

decreases by only 20% at $T < T_N$ [Fig. 11(a)]. As the temperature increases [Figs. 11(b) and 11(c)], the resistance in the IR range increases owing to a recombination of electrons and holes and, in the visible spectral range, remains almost invariable at the long-term exposure.

To explain the observed effects, we present the electron spectrum, which includes the valence and conduction bands, impurity subband, and donor level in the low- and high-temperature regions [Figs. 12(a) and 12(b)]. Below 200 K, the impurity band is split due to the interaction between spins of localized and delocalized electrons [Fig. 12(a)], which affects the transport properties. Above 200 K, the impurity subband narrows and lies above the chemical potential and the transport properties are determined by the transition from the valence to impurity band of holes with $E_a = 0.14\text{ eV}$, which was found from the $\log \rho(1/T)$ dependence. Under the IR irradiation, the electrons pass from the donor level to the valence band with an increase in temperature, which leads to the carrier recombination.

IV. CONCLUSIONS

The cationic substitution of silver for manganese in the $\text{Ag}_x\text{Mn}_{1-x}\text{S}$ system induces a set of magnetoresistance, magnetoimpedance, magnetothermopower, and photoconductivity effects. Near the magnetic phase transition, the maximum decrease in the electrical resistance and impedance in a magnetic field was found. Below the Neel temperature, the $\text{Ag}_{0.05}\text{Mn}_{0.95}\text{S}$ sample exhibits the anomalous behavior of magnetization caused by the formation of ferromagnetic droplets (ferrons) in the antiferromagnetic matrix. The formation of ferrons near the magnetic transition temperature was confirmed by the IR spectroscopy data and $I\text{--}V$ characteristic nonlinearity, which vanishes with an increase in temperature and magnetic field.

A study of the impedance spectra showed the existence of several conductivity channels. The relaxation time was determined from the frequency dependence of the active and reactive resistances, which are described in the framework of the Debye model. Above the temperature of the magnetic transition, the hole density and mobility were obtained. The change in the thermopower sign upon temperature variation is caused by dragging carriers by magnons, which disappear in the paramagnetic region.

In the magnetically ordered region, the electromagnetic radiation absorption was found in the IR range, which vanishes above the Neel temperature. The dependence of the resistance on the IR and visible illumination at different temperatures was obtained. The experimental data were explained using the spin-polaron model. Below 200 K, the impurity subband is split due to the interaction of spins of localized and delocalized electrons. With an increase in temperature, the impurity subband narrows and lies above the chemical potential and the transport properties are determined by the transition from the valence to the impurity band of holes.

ACKNOWLEDGMENTS

This study was supported by the Russian Foundation for Basic Research (Project No. 18-52-00009 Bel_a). The reported study was funded by the Russian Foundation for Basic Research, Government of Krasnoyarsk Territory, Krasnoyarsk Regional Fund of Science

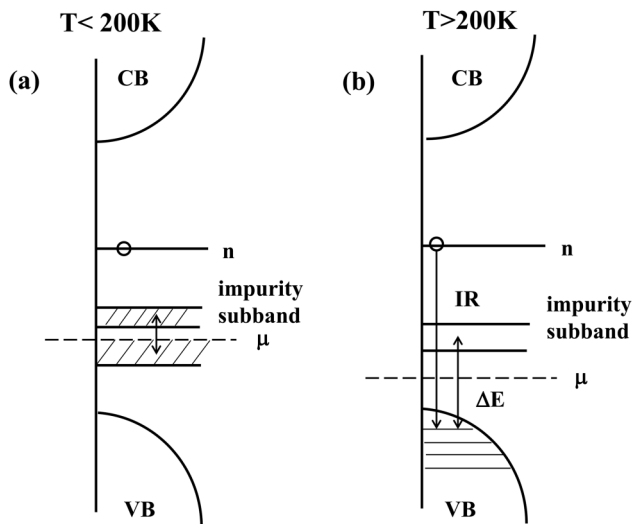


FIG. 12. State density diagram of the $\text{Ag}_{0.05}\text{Mn}_{0.95}\text{S}$ solid solution in the temperature ranges of (a) $T < 200\text{ K}$ and (b) $T > 200\text{ K}$. CB is the conduction band, VB is the valence band, μ is the chemical potential, n is the donor level, and IR is the irradiation.

(Project No. 18-42-240001 r_a), to the research project: “Inversion of the Sign of the Components of the Magnetoelectric Tensor on the Temperature in Films of Bismuth Garnet Ferrite Replaced by Neodymium.” This study was carried out in the framework of the state task No. 3.5743.2017/6.7.

REFERENCES

- ¹A. Fert, *Rev. Mod. Phys.* **80**, 1517 (2008).
- ²N. V. Volkov, *Usp. Fiz. Nauk* **182**, 263 (2012).
- ³A. Kumar, C. V. Tomy, and A. D. Thakur, *Mater. Res. Express* **5**, 086110 (2018).
- ⁴A. J. Millis, B. I. Shraiman, and R. Mueller, *Phys. Rev. Lett.* **77**, 175 (1996).
- ⁵A. Kumar, C. V. Tomy, and A. D. Thakur, *Mater. Res. Express* **5**, 086110 (2018).
- ⁶S. S. Aplesnin, L. I. Ryabinkina, O. B. Romanova, D. A. Balaev, O. F. Demidenko, K. I. Yanushkevich, and N. S. Miroshnichenko, *Phys. Solid State* **49**, 2080 (2007).
- ⁷R. Xu, A. Husmann, T. F. Rosenbaum, M.-L. Saboungi, J. E. Enderby, and P. B. Littlewood, *Nature* **390**, 57 (1997).
- ⁸D. Kriegner, K. Výborný, K. Olejník, H. Reichlová, V. Novák, X. Marti, J. Gazquez, V. Saidl, P. Němec, V. V. Volobuev, G. Springholz, V. Holý, and T. Jungwirth, *Nat. Commun.* **7**, 11623 (2016).
- ⁹S. S. Aplesnin, O. B. Romanova, and K. I. Yanushkevich, *Phys. Status Solidi (b)* **252**, 1792 (2015).
- ¹⁰S. M. Alekperova, I. A. Akhmedov, G. S. Gadzhieva, and K. D. Dzhalilova, *Phys. Solid State* **49**, 512 (2007).
- ¹¹S. S. Aplesnin, L. I. Ryabinkina, O. B. Romanova, D. A. Velikanov, A. D. Balaev, K. I. Yanushkevich, A. I. Galyas, O. F. Demidenko, and O. N. Bandurina, *J. Exp. Theor. Phys.* **106**, 765 (2008).
- ¹²S. S. Aplesnin, M. N. Sitnikov, O. B. Romanova, and A. Y. Pichugin, *Phys. Status Solidi (b)* **253**, 1771 (2016).
- ¹³R. G. Lalitha, L. Y. Kalyana, K. N. Pavan, R. S. Manjunath, and R. P. Venugopal, *J. Magn. Magn. Mater.* **362**, 20 (2014).
- ¹⁴D. Salazar, D. Arias, O. J. Durá, and M. A. López de la Torre, *J. Alloys Comp.* **583**, 141 (2014).
- ¹⁵D. V. Macheswar Repaka and R. Mahendiran, *J. Appl. Phys. Lett.* **103**, 162408 (2013).
- ¹⁶S. Sagar, V. Ganesan, P. A. Joy, S. Thomas, A. Liebig, M. Albrecht, and M. R. Anantharaman, *Europhys. Lett.* **91**, 17008 (2010).
- ¹⁷D. Berthebaud, O. I. Lebedev, A. Maignan, and S. Hebert, *J. Appl. Phys.* **124**, 063905 (2018).
- ¹⁸H. H. Heikens, C. F. van Bruggen, and C. Haa, *J. Phys. Chem. Soc.* **39**, 833 (1978).
- ¹⁹E. L. Nagaev, *Physics of Magnetic Semiconductors* (Nauka, Moscow, 1979), p. 431 (in Russian).
- ²⁰H. H. Heikens, G. A. Wiegers, and C. F. van Bruggen, *Solid State Commun.* **24**, 205 (1977).
- ²¹S. S. Aplesnin, G. A. Petrakovskii, L. I. Ryabinkina, G. M. Abramova, N. I. Kiselev, and O. B. Romanova, *Solid State Commun.* **129**, 195 (2004).
- ²²S. S. Aplesnin, L. I. Ryabinkina, G. M. Abramova, O. B. Romanova, A. M. Vorotynov, D. A. Velikanov, N. I. Kiselev, and A. D. Balaev, *Phys. Rev. B* **71**, 125204 (2005).
- ²³E. L. Nagaev, *Usp. Fiz. Nauk* **39**, 781 (1996).
- ²⁴S. I. Sadovnikov, *A.I. Gusev Phys. Sol. St.* **59**, 1887 (2017).
- ²⁵G. A. Petrakovskii, L. I. Ryabinkina, G. M. Abramova, A. D. Balaev, O. B. Romanova, G. I. Makovetskii, K. I. Yanushkevich, and A. I. Galyas, *Phys. Solid State* **44**, 1925 (2002).
- ²⁶J. S. Smart, *J. Phys. Chem. Solids* **11**, 97 (1959).
- ²⁷M. Y. Kagan and K. I. Kugel, *Usp. Fiz. Nauk* **171**, 577 (2001).
- ²⁸N. P. Stepina, E. S. Koptev, A. G. Pogosov, A. V. Dvurechenskii, A. I. Nikiforov, E. Y. Zhdanov, and Y. M. Galperin, *J. Phys. Condens. Matter.* **25**, 505801 (2013).
- ²⁹B. Kochman, S. Ghosh, J. Singh, and P. Bhattacharya, *J. Phys. D Appl. Phys.* **35**, L65 (2002).
- ³⁰C. M. Hurd, *The Hall Effect in Metal and Alloys* (Plenum Press, New York, 1972), p. 400.